Rev. Adv. Mater. Sci. 57 (2018) 167-174

PREPARATION OF TRANSPARENT n-ZnO:Al / p-$CuAlCrO_2$ HETEROJUNCTION DIODE BY SOL-GEL TECHNOLOGY

E.V. Shirshneva-Vaschenko[1], L.A. Sokura[1,2], P.S. Shirshnev[1], D.A. Kirilenko[1,2], Zh.G. Snezhnaia[1], D.A. Bauman[1], V.E. Bougrov[1] and A.E. Romanov[1,2]

[1]ITMO University, Kronverkskiy prospect 49, Saint-Petersburg, 197101, Russia
[2]Ioffe Institute, Polytechnicheskaya 26, Saint-Petersburg, 194021, Russia

Received: May 11, 2018

Abstract. This paper presents the study of oxide film heterojunction made of $CuAlCrO_2$ and ZnO:Al (AZO) deposited on fused quartz by sol-gel spin coating. Transmission electron microscopy (TEM) analysis has showed that the solvent, which was used to prepare the AZO sol, affects the thickness and planarity of the applied layers and the grain size of the polycrystalline film. The formation of a fine-grained structure of AZO films (grain size is up to 12 nm) leads to the formation of a smoother p-$CuAlCrO_2$ / n-AZO heterojunction. X-ray diffraction (XRD) analysis and TEM have revealed that the heterojunction was formed by AZO polycrystals, which orient axes [101] and [100] against the [101] and [006] directions in $CuAlCrO_2$ polycrystals. The optical transmission of the heterojunction in the visible range reached 70 %. The current –voltage (I-V) characteristics of p-$CuAlCrO_2$ / n-AZO corresponds to a diode one in the range from 4 up to 4 V. For the large values of the reverse bias, an increase in the leakage current is observed, which is associated with tunneling breakdown of heterojunction. The ideality factor of fabricated p-$CuAlCrO_2$ / n-AZO heterojunction is more than 2, which indicates the mechanisms of conductivity by defect-levels. In additional, it has been observed the response of the current-voltage characteristics to the green illumination (532 nm) of the diode that is associated with indirect band-gap absorption in $CuAlCrO_2$. The impact of the white LED illumination had no effect on the current-voltage characteristics of the diode.

1. INTRODUCTION

To fabricate a transparent in the visible spectral range heterojunction, it is necessary to have n-type and p-type semiconductors with band gap, which is more than 3 eV. Such materials as transparent conductive oxides (TCOs) are very suitable for this function. TCOs themselves are mostly n-type semiconductors. Design and fabrication of p-type TCO with good band alignment to n-TCO is the main task for obtaining the transparent p-n junction [1]. The materials with delaffosite structure are preferable to p-TCO [2]. Nickel oxide (NiO) is a second important matter for the formation of a heterojunction [3]. To observe the current flow through the p – n junction, a good agreement of the lattice parameters of two materials is necessary. However, in [4] it was demonstrated that the current-voltage characteristics of the device corresponds to the diode one for the p-$SrCu_2O_4$ / n-ZnO heterojunction with rather large mismatch of the lattice parameters. This result initiated the research in the area of oxide heterojunctions and provided an opportunity for fabricating structures by various techniques.

In the works on fabrication of heterojunctions based on TCOs, the authors mainly use the following coating techniques: pulsed laser deposition technique [5-10], magnetron sputtering [11-13], plasma-enhanced metal-organic CVD (PE-MOCVD) [14,15].

Corresponding author: E.V. Shirshneva-Vaschenko, e-mail: elena.vaschenko@niuitmo.ru

The application of vacuum and technologically complex methods is caused by the necessity to obtain a good interface of heterojunction [16]. Electrochemical deposition [17-19] and sol-gel [20-22] methods are alternative non-vacuum processes for low-cost, high throughput thin film deposition.

In the scientific community, there is a limited number of publication related to oxide heterojunctions fabrication using solution chemistry methods. In these works on transparent oxide heterojunctions fabrication by the sol-gel method, NiO is generally used as the p -layer due to its simple structure and composition [21,22]. As a rule, only n-layer is prepared by chemical methods [23].

In this work, zinc oxide doped with aluminum (AZO) as the n-layer and chromium doped $CuAlO_2$ as the p-layer of heterojunction were selected. Both layers are prepared using the sol-gel method of spin-coated deposition. This is the first work in the sphere of fabrication a p-n junction by the sol – gel method, where the p-type layer has a delaffosite structure.

The band arrangement of p- and n-type oxides plays a crucial role for the formation of the heterojunction. An electron affinity and band gap values of $CuAlCrO_2$ [24] are closer to AZO parameters than NiO values. Thus, the band offsets in the p-$CuAlCrO_2$ / n-AZO pair are smaller than in the p-NiO / n-AZO pair. Moreover delaffosites have a hexagonal structure, like AZO, thereby are more preferable to obtain good interface. These two factors have determined the choice of $CuAlCrO_2$ as a pair for AZO.

In the previous works [25,26] the authors obtained transparent conductive oxides of n- and p-type conductivity: AZO and $CuAlCrO_2$ by the sol-gel method. The parameters of the fabricated films are the following: for AZO electrical resistivity is 0.3 Ω cm and optical transmittance in the visible region is up to 90%. For $CuAlCrO_2$ electrical resistivity is 4 k Ω cm and optical transmittance in the visible region is up to 70 %.

2. FABRICATION OF p-$CuAlCrO_2$ / n-AZO HETEROJUNCTION

For this research, two types of p-$CuAlCrO_2$ / n-AZO heterojunctions, which had different solvents for the n-layer preparation, were used. For the first (Sample 1) and the second (Sample 2) type of heterojunctions fabrications ethanol and 2-Methoxyethanol were used for n-layer preparing respectively.

To fabricate a p-n heterojunction, ten monolayers of $CuAlCrO_2$ were deposited on a fused quartz substrate. After annealing, a mask covering the part of the prepared $CuAlCrO_2$ film was deposited, and then monolayers of AZO were deposited on the top of the structure. Sample 1 and Sample 2 differ in number of AZO monolayers, three monolayers and ten monolayers consequently. For current-voltage characteristics measurements, silver electrodes were deposited on the surfaces of $CuAlCrO_2$ and AZO.

The sol solution for AZO consisted of zinc acetate dehydrate [$Zn(O_2CCH_3)_2$, ZnAc] and aluminum nitrate [$Al(NO_3)_3$] was dissolved in ethanol (2-Methoexyethanol) with concentration of 0.4 M (0.2 M). Monoethanolamine (MEA) was used as a stabilizer. The molar ratio of MEA/ZnAc was 1:1. The molar ratio of Zn/Al was 1:0.03. The film was annealed in air for 1 hour at 600 °C [25].

The sol solution for $CuAlCrO_2$ films precursor solution consisted of $Cu(CH_3COO)_2 \cdot H_2O$ + $Al(NO_3)_3 \cdot 9H_2O$ + $Cr(NO_3)_3 \cdot 9H_2O$ and was dissolved in 2-Methoexyethanol. The molar ratio of Cu/Al/Cr was 1:0.5:0.5. The concentration of solution was 0.2 M. The film was annealed in air for 1 hour at 950 C [26].

3. CHARACTERIZATION

The morphology of p-$CuAlCrO_2$ / n-AZO heterojunctions (Sample 1, Sample 2) was determined through transmission electron microscope (TEM) technique using a JEOL JEM-2100F with the accelerating voltage of 200 keV. The samples were prepared in a cross section in accordance with the standard procedure, including preliminary mechanical thinning and further polishing with an ion beam (argon ion beam energy - 4 keV). Samples were examined in diffraction and high resolution modes.

Phase identification and crystallographic structure determination were realized using X-ray diffraction (XRD) on a Dron-8 X-ray diffractometer with $CuK\alpha_1$ radiation (40 kV, 20 mA, λ = 0.154056 nm) in the 2θ range of 10-95°. The optical transmission spectra measurements were performed with the fiber spectrometer AvaSpec-2048. The I-V measurements were recorded by sourcemeter (Keithley 2450) in the darkness and with illumination of green diode light at 532 nm. The ohmic behavior of the electrodes was verified by I-V measurements between two silver contacts on the surfaces of $CuAlCrO_2$ and AZO.

4. RESULTS AND DISCUSSION

4.1. Morphological analysis

The morphology of the samples (Sample 1, Sample 2) as well as of n-AZO and p-$CuAlCrO_2$ layers on fused quartz substrates was determined through a

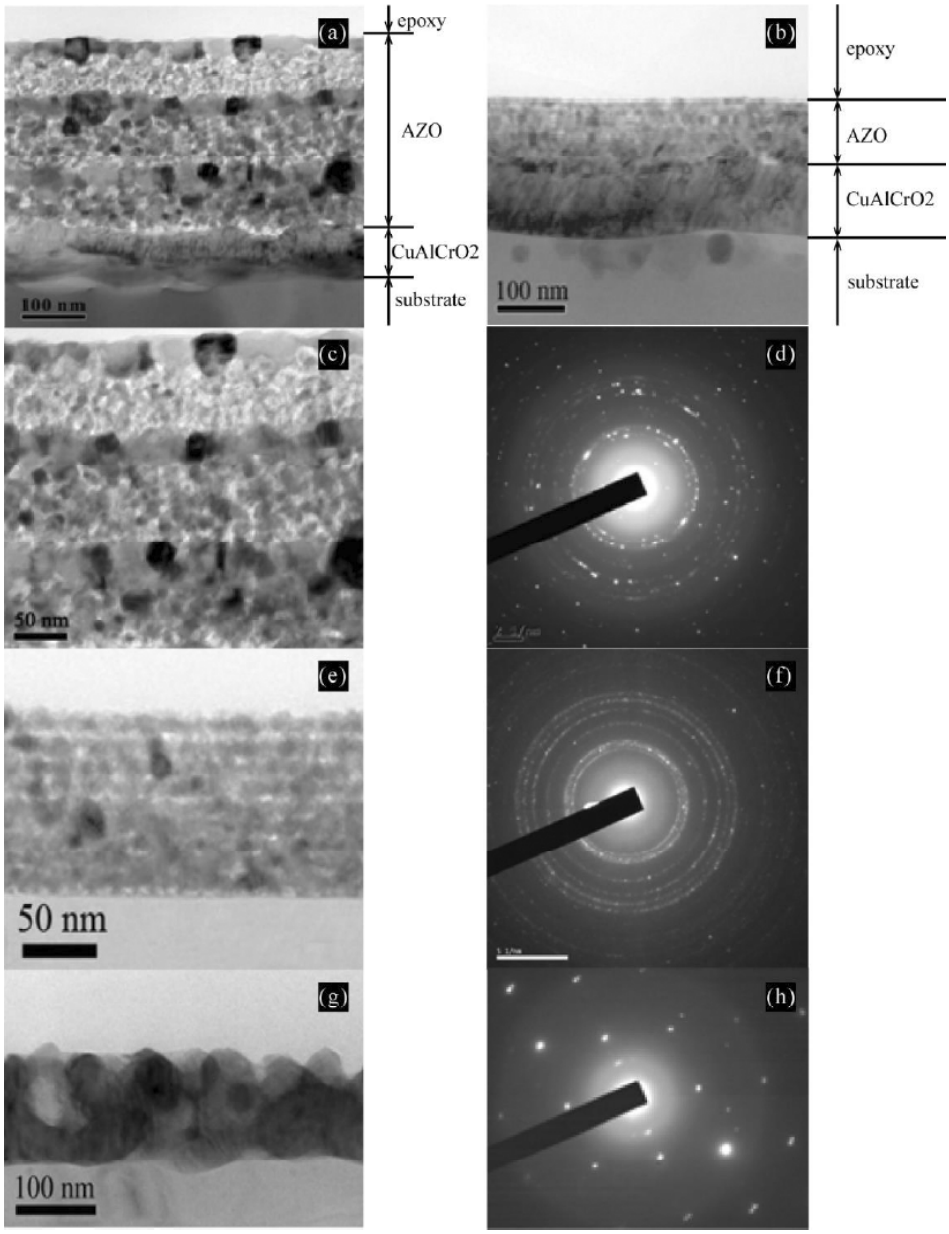

Fig. 1. a) Cross section TEM image of Sample 1 (n-AZO (ethanol) / p-CuAlCrO$_2$); b) cross section TEM image of Sample 2 (n-AZO (2-Methoxyethanol) / p-CuAlCrO$_2$; c) cross section TEM image of layer n-AZO (ethanol); d) diffraction pattern of layer n-AZO (ethanol); e) cross section TEM image of layer n-AZO (2-Methoxyethanol); f) diffraction pattern of layer n-AZO (2-Methoxyethanol); g) cross section TEM image of layer p-CuAlCrO$_2$; h) diffraction pattern of layer p-CuAlCrO$_2$.

transmission electron microscopy technique. Figs. 1a-1h present the cross section TEM images of Sample 1 and 2, the cross section TEM images of n-AZO, and p-CuAlCrO$_2$ layers, and diffraction patterns for n-AZO and p-CuAlCrO$_2$ layers.

From Figs. 1a and 1b, it can be seen that the planarity of the boundary between the AZO layer and CuAlCrO$_2$ is disturbed in both cases. However, the interface between the layers is smoother in Sample 2. Fig. 1c shows the cross section TEM image of n-AZO layer prepared from a sol based on ethanol solution. The total thickness of the layer is from 250 to 280 nm. In the AZO layer, we observe three coarse-grained monolayers separated by fine-grained ones. The small grains are up to 10 nm, while the large ones reach 30 nm. The diffraction pattern (Fig. 1d) corresponds to a polycrystalline sample. Fig. 1e presents the cross section TEM images of n-AZO layer prepared from a sol-based on 2-Methoxyethanol solution. The total thickness of the layer is from 82 up to 87 nm. The separate monolayers with grains from 9 to 12 nm in size are

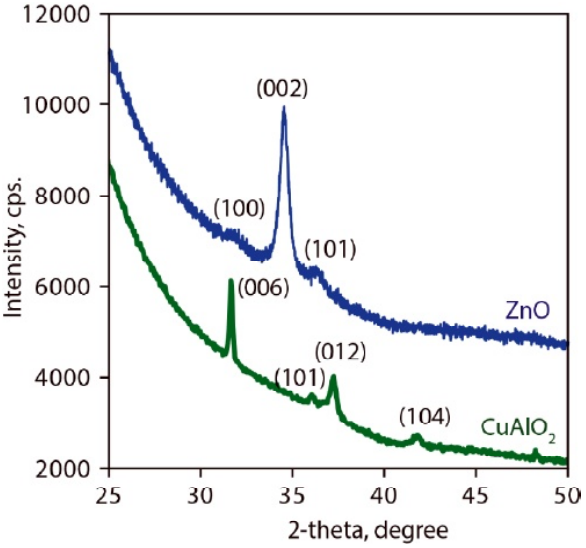

Fig. 2. XRD patterns of: p-$CuAlCrO_2$ layer on fused quartz substrate (red curve); n-AZO layer on fused quartz substrate (blue curve).

clearly observed. Fig. 1g represents the cross section TEM images of a p-$CuAlCrO_2$ layer on a fused silica substrate. The total film thickness of the layer is from 75 to 85 nm, the size of one grain is from 50 to 75 nm. The grain misorientation angle in the $CuAlCrO_2$ layers is only 1.5–2 degrees, which determines by the point diffraction pattern with a slight stretching of the reflexes in arcs (Fig. 1h).

4.2. Structural characterization

The phases of the p-$CuAlCrO_2$ / n-AZO heterojunction components were confirmed with XRD measurements as shown in Fig. 2.

To calculate the XRD patterns of the samples, the positions of the diffraction peaks were determined and the relative integrated intensity was calculated. The calculation of interplanar distances were determined according to the Bragg's formula [27]:

$$2d \sin\theta = n\lambda,$$

where n - an order of diffraction maximumo, λ - the wavelength of the X-ray, d - is the distance between the lattice plane, θ - is the incident angle (Bragg angle).

The particles size was determined by the Scherrer formula [28] on the basis of the position and intensity at the half width (FHWM) of diffraction maxima:

$$l = \frac{R * \lambda}{\beta * \cos\theta},$$

where l - the linear particles size and R - a numerical constant.

In the p-type layer, the crystalline phase is $CuAlO_2$ (Fig. 2, red): its spatial group is R-3m (166) and has hexagonal syngony. Chromium doping appears as a weak peak displacement. The calculated lattice constants for the p-$CuAlCrO_2$ are a = 2.907 Å, b = 2.907 Å, c = 16.960 Å (α = 90°, β = 90°, γ = 120°). The average crystal size calculated by the Scherrer formula is about 30 nm.

In the n-type layer, the crystalline phase is ZnO (Fig. 2, blue). The spatial group of this phase is P63mc (186); it has hexagonal syngony. Aluminum doping is manifested as a weak peak displacement. The calculated lattice constants for the n-AZO are a = 3.242 Å, b = 3.242 Å, c = 5.195 Å (α = 90°, β = 90°, γ = 120°). The average crystal size, calculated using the Scherrer formula, is about 11 nm.

Both ZnO and $CuAlO_2$ have the hexagonal lattice type. The interplanar distances in the [101] direction for ZnO and $CuAlO_2$ are the same and in the [100] direction for ZnO and in the [006] direction for $CuAlO_2$ are also the same. In all these cases, the interplanar distances have a mismatch less than 1%. Therefore, during the formation of layers, the polycrystals of the ZnO layer are oriented by the [101] and [100] axes against the [101] and the [006] directions of $CuAlO_2$. From the TEM images it can be seen that the [006] axis of $CuAlO_2$ is in the plane of the substrate.

The formation of smaller grain size of AZO prepared from 2-Methoexyethanol solution simplifies the embedding of AZO grains on the polycrystalline $CuAlO_2$ layer and leads to the formation of a smoother heterointerface.

4.3. Optical characterization

The transmittance spectra with the wavelength from 300 to 1000 nm of Sample1 and Sample 2 are shown in Figs. 3a and 3b. From Fig. 3b it can be seen that the optical transmittance for Sample 2 reaches up to 70% in visible region. The optical transmittance of Sample 1 is less than 40% in the visible region that indicates the shadow of the sample on interface and, consequently, bad heterojunction formation.

4.4. Current-voltage characteristics of p-$CuAlCrO_2$ / n-AZO heterojunction

The band offsets between n- and p-layers are important properties of heterostructure. To construct

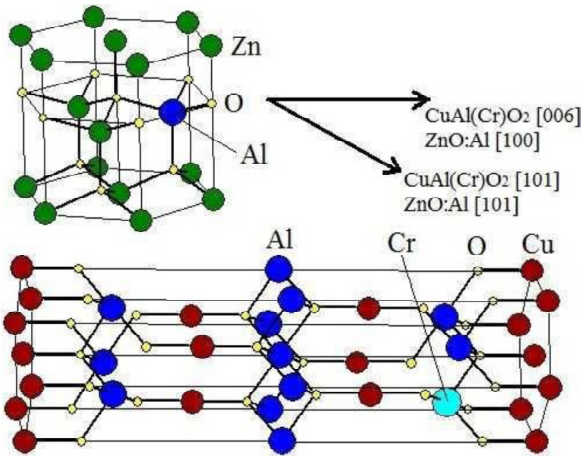

Fig. 3. Schematic representation of the ZnO and $CuAlO_2$ crystal structures and their relative orientations.

the band diagram of the heterojunction, the Anderson model [29] is used. The band offset of the conduction bands in p-$CuAlCrO_2$ and in n-AZO, the band offset of the valence bands in p-$CuAlCrO_2$ and in n-AZO are 1.8 eV and 1.9 eV, respectively. In our calculations, it was taken into account that the values of the electron affinity for materials are 2.44-2.54 eV for $CuAlCrO_2$ [30,31] and 4.2-4.6 eV for AZO [32,33]. The values of the band gaps measured in the previous works were 3.17 eV for $CuAlCrO_2$ [25] and 3.3 eV for AZO [26]. Based on the values of electrical parameters for $CuAlCrO_2$ and AZO [34-36], the positions of the Fermi levels and the contact potential difference for materials were determined. The band diagram for p-$CuAlCrO_2$/ n-AZO heterojunction is demonstrated in Fig. 4.

The performance of the prepared heterojunctions (Sample 1, Sample 2) was investigated using the current-voltage characterization. Fig. 5 shows the current-voltage characteristics of Sample 2 in the darkness at the room temperature. From Fig. 5 it can be seen that heterostructure provides nonlinear behavior, confirming the p-n heterojunction formation. Sample 1 provides the linear behavior of current-voltage characteristics and, considering the observed bad optical transmittance for this sample, we can confirm the absence of heterojunction.

Increased current is observed on green light (532 nm) exposure under both forward and reverse bias (Fig. 5a, green curve), indicating the photo responsive nature of p-$CuAlCrO_2$/ n-AZO heterojunction. These current enhancements reveal the absorption of incident green light by the p-$CuAlCrO_2$ layer and further generation of photocarriers by excitation of electrons from the taps levels of Cu in band gap to conduction band [36].

Fig. 6 shows the current-voltage characteristics of the current density in the range from -6 up to 6 volts. It can be seen that when reserve bias is greater than 4 V, there is a sharp increase in leakage current associated with tunneling breakdown.

The ideality factor of the diodes is determined by assuming the Shockley equation [37]:

$$I = I_s\left[\exp\left(\frac{qU}{\eta k_B T}\right) - 1\right],$$

where q – an elementary charge, U – the applied voltage, k_B – the Boltzmann constant, T – the temperature, I_s – the saturation current. Therefore, the

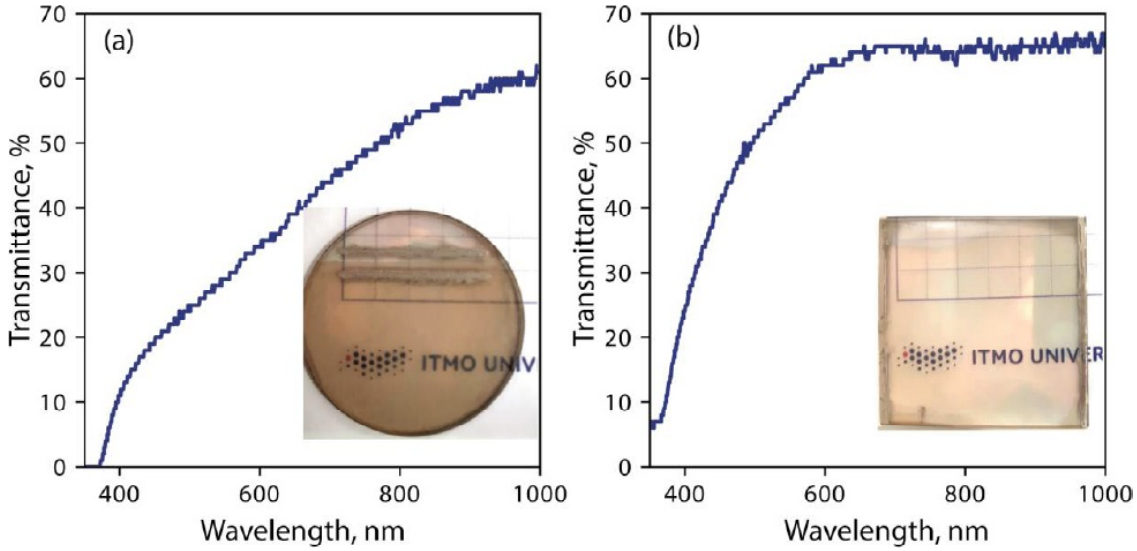

Fig. 4. Transmittance spectra of heterojunctions samples: a) Sample 1 (n-ZnO:Al (ethanol)/p-$CuAlCrO_2$); b) Sample 2 (n-ZnO:Al (2-Methoxyethanol)/p-$CuAlCrO_2$). Inset: the images of fabricated samples.

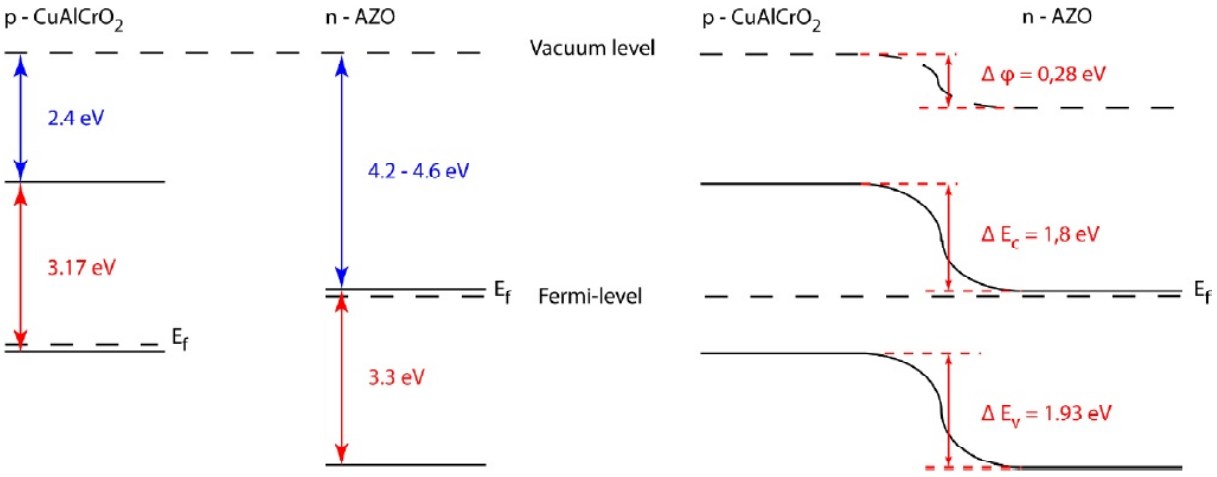

Fig. 5. Band energy diagram of the isolated n-AZO, p-$CuAlCrO_2$ layers and heterojunction under equilibrium condition.

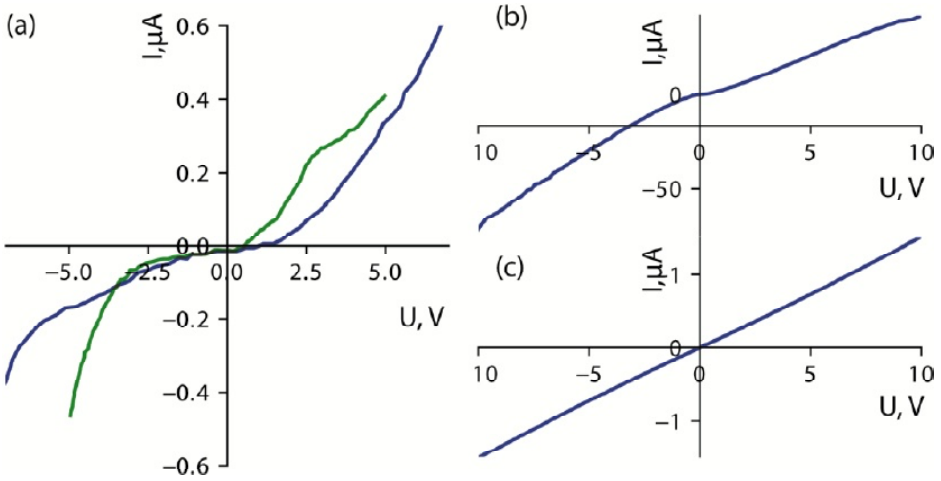

Fig. 6. a) Current-voltage characteristic of p-$CuAlCrO_2$/n-AZO heterojunction (Sample 2): (black) in the dark; (red) under green light illumination 532 nm. b) *I-V* linear characteristic of AZO/Ag contact; c) *I-V* linear characteristic of $CuAlCrO_2$/Ag contact.

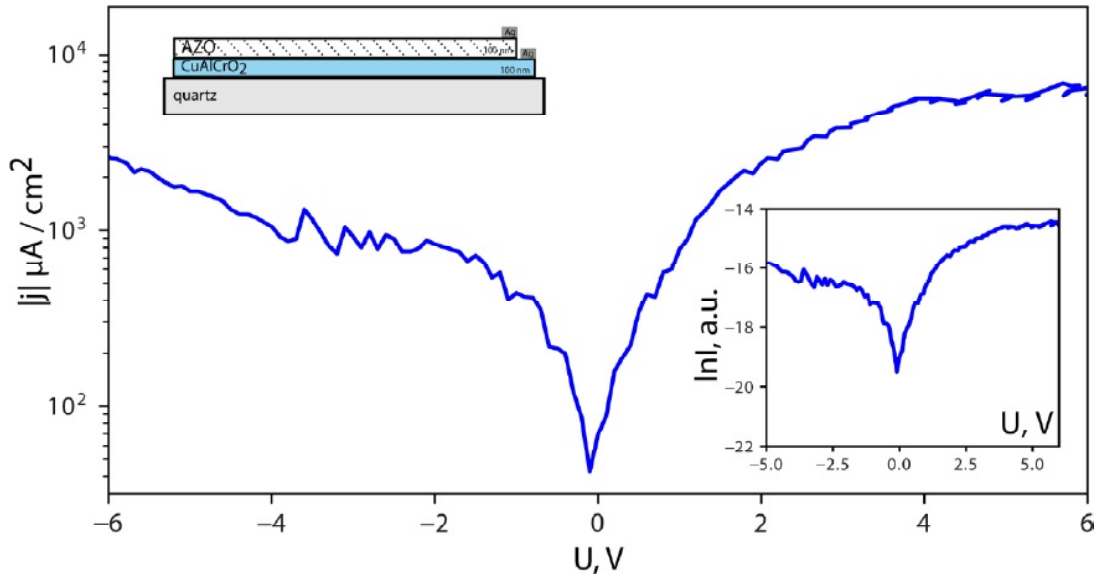

Fig. 7. The current-voltage characteristic of the current density in the range from -6 up to 6 volts. The inset illustrates a schematic cross section of the p-$CuAlCrO_2$/n-AZO heterojunction. The inset graph show ln*I* versus *V* characteristic.

ideality factor of the diodes is determined from the slope ln*I* to *U* with a positive forward bias.

A linear fit in a ln*I* versus *V* plot results in η=4 for forward bias up to 0.5 V. The ideality factor increases together the voltage with. The ideality factor greater than 2 was observed in studies of wide-gap oxide heterojunctions and homojunctions [38, 39]. The great value of the ideality factor is related to the influence on the current flow process through the heterojunction of the following mechanisms: the presence of the surface or interface states, the defect-level recombination, and the space-charge limited conduction [40].

Despite the fact that polycrystalline layers lead to the presence of a large number of inhomogeneities and defect states at interface of heterojunction, we suppose that using the sol-gel method to diode fabrication is justified. It is also assumed that the adding of buffer layers into the heterojunction structure and the variation of dopant concentrations in the layers will reduce the ideality factor of the heterojunction transition. An annealing in inert gases prepared by the sol-gel layers method will lead to an interface improvement and therefore to the improvement in diode characteristics.

5. CONCLUSIONS

We have demonstrated the facile fabrication by sol-gel technology of transparent diode on p-$CuAlCrO_2$ / n-AZO heterojunction. It has been shown that the formation of a fine-grained structure in the AZO layers makes it possible to fabricate a good heterointerface and leads to diode formation. The combined analysis of TEM and XRD measurements has indicated that the layers have all prerequisites for the heterojunction formation. The orientation of the $CuAlCrO_2$ polycrystals on the fused quartz substrate allows the AZO polycrystals to form a layer along the directions with minimal mismatch of interplanar distances. The optical transmission of the heterojunction in the visible range reaches 70%. The current-voltage characteristics corresponds to a diode with the ideality factor of 4, associated with defective formations at the boundaries. The task of improving the current-voltage characteristics of the p-$CuAlCrO_2$ / n-AZO heterojunction is promising in devices fabricated on the base of the solution chemistry method.

ACKNOWLEDGEMENT

This work was supported by the Ministry of Education and Science of the Russian Federation in the framework of the Federal Target Program “Research and development in priority directions of the scientific-technological complex of Russia for 2014-2020”, code 2017-14-576-0003, agreement № 14.575.21.0127 from September 26, 2017, unique ID RFMEFI57517X0127.

REFERENCES

[1] H. Hosono // *Thin solid films* **515** (2007) 6000.
[2] H. Kawazoe, H. Yanagi, K. Ueda and H. Hosono // *MRS Bulletin* **25** (2000) 28.
[3] H. Sato, T. Minami, S. Takata and T. Yamada // *Thin solid films* **236** (1993) 27.
[4] A. Kudo and H. Yanagi // *Appl phys let* **75** (1999) 2851.
[5] K. Tonooka, H. Bando and Y. Aiura // *Thin Solid Films* **445** (2003) 327.
[6] H. Ohta, M. Kamiya, T. Kamiya, M. Hirano and H. Hosono // *Thin Solid Films* **445** (2003) 317.
[7] H. Yanagi, K. Ueda, H. Ohta, M. Orita and M. Hirano // *Solid state communications* **121** (2001) 15.
[8] H. Tanaka, T. Shimakawa, T. Miyata, H. Sato and T. Minami // *Thin solid films* **469** (2004) 80.
[9] W. Siripala, A. Ivanovskaya, T. F. Jaramillo, S. H. Baeck and E. W. McFarland // *Solar Energy Materials and Solar Cells* **77** (2003) 229.
[10] H. Ohta, M. Hirano, K. Nakahara, H. Maruta, T. Tanabe, M. Kamiya and H. Hosono // *Applied physics letters* **83** (2003) 1029.
[11] R.E. Stauber and J.D. Perkins // *Solid-state let* **2** (1999) 654.
[12] K. C. Sanal and M. K. Jayaraj // *Materials Science and Engineering: B* **178** (2013) 816.
[13] B. Ling, X. W. Sun, J. L. Zhao, S. T. Tan and Z.L. Dong // *Physica E: Low-dimensional Systems and Nanostructures* **41** (2009) 635.
[14] Y. Wang and H. Gong // Adv. Mater CVD **6** (2000) 285.
[15] H. Ohta, H. Mizoguchi, M. Hirano, S. Narushima, T. Kamiya and H. Hosono // *Applied physics letters* **82** (2003) 823.
[16] T. Minami, T. Miyata, K. Ihara, Y. Minamino, S. Tsukada and T. Minami // *Thin Solid Films* **494** (2006) 47.
[17] H. Lahmar, F. Setifi, A. Azizi, G. Schmerber and A. Dinia // *Journal of Alloys and Compounds* **718** (2017) 36.

[18] M. Izaki, T. Shinagawa, K.T. Mizuno, Y. Ida, M. Inaba and A. Tasaka // *Journal of Physics D: Applied Physics* **40** (2007) 3326.
[19] M. Pavan, S. Rühle, A. Ginsburg, D. A. Keller, H. N. Barad and P. M. Sberna // *Solar Energy Materials and Solar Cells* **132** (2015) 549.
[21] X. Chen // *Applied Physics Letters* **93** (2008) 112112.
[22] N. Park // *Journal of Materials Chemistry C* **1** (2013) 7333.
[23] B. V. Mistry // *Thin Solid Films* **519** (2011) 3840.
[24] S. Y. Tsai, M. H. Hon and Y. M. Lu // *Solid-State Electronics* **63** (2011) 37.
[25] E. V. Shirshneva-Vaschenko // *Materials Physics and Mechanics* **29** (2016) 145.
[26] E. V. Shirshneva-Vaschenko // *Materials Physics and Mechanics* **32** (2017) 288.
[27] L. R. B. Elton and F. Daphne // *American Journal of Physics* **34** (1966) 1036.
[28] A. L. Patterson // *Physical review* **56** (1939) 978.
[29] A. G. Milnes and D. L. Feucht, *Heterojunctions and Metal Semiconductor Junctions* (Academic, New York, 1972).
[30] Z. Q. Yao // *Applied Physics Letters* **100** (2012) 062102.
[31] W. Suzhen// Journal of Semiconductors **35** (2014) 043001.
[32] U. N. Roy // *Scientific reports* **6** (2016) 26384.
[33] L. Zhu, G. Shao and J. K. Luo // *Semiconductor Science and Technology* **26** (2011) 085026.
[34] D. S. Kim // *Physica status solidi (a)* **203** (2006) R51.
[35] A. N. Banerjee and K. K. Chattopadhyay // *Progress in Crystal Growth and Characterization of materials* **50** (2005) 52.
[36] A. N. Banerjee, S. Nandy, C. K. Ghosh and K. K. Chattopadhyay // *Thin Solid Films* **515** (2007) 7324.
[37] C. T. Sah, R. N. Noyce and W. Shockley // *Proceedings of the IRE* **45** (1957) 1228.
[38] F. L. Schein, H. von Wenckstern and M. Grundmann // *Applied Physics Letters* **102** (2013) 092109.
[39] R. S. Ajimsha, K. A. Vanaja, M. K. Jayaraj and P. Misra // *Thin Solid Films* **515** (2007) 7352.
[40] M. A. Lampert, P. Mark, *Current injection in solids* (NY: Academic Press, 1970).